ICAS Proceeding 1994, Anaheim/USA
Vol. 1, 801-812.

AERODYNAMICS OF A SLENDER WING WITH VERTICAL FINS AT LOW SPEED

Prof. Dr.-Ing. Dietrich Hummel
Dipl.-Ing. Andreas Brümmer
Institut für Strömungsmechanik
TU Braunschweig, Bienroder Weg 3
D - 38106 Braunschweig, Germany

Abstract

Wing-fin interference has been investigated at low speed for a cropped delta wing (aspect ratio A = 0.93, taper ratio λ = 0.33, leading-edge sweep φ = 65°) as the vortex generator and half-wing-shaped vertical fins of different size. Single fins in the symmetry plane of the configuration as well as double fins at mid semispan and at the wing tips have been investigated. Six-component balance and pressure distribution measurements have been carried out. In addition the flow has been studied using the Laser ligthsheet technique, by means of probe measurements in the flowfield as well as by visualization of the surface flow using oilflow patterns.

A central fin is less effective than double fins of the same total area located at the wing tips. Double fins at mid semispan are extremely unfavourable since an instability of the lateral motion takes place within a certain angle of attack range. At high angles of attack and unsymmetrical flow sudden and considerable changes of the aerodynamic coefficients occur for central single fins and mid semispan double fins. The vortex-induced crossflow causes the formation of fin vortices, and the disturbance of the wing vortex flow by the presence of the fins leads to increased wing vortex breakdown. Double fins at the wing tips are favourable configurations and the vortex formation on these fins can be used to increase their effectiveness.

1. Introduction

For generic hypersonic flight vehicles as well as for many fighter aircraft slender wing-body combinations are used which are stabilized in the whole Mach number range by means of fins. During landing at low speed and high angles of attack the flowfield over such configurations is governed by a pair of vortices which is generated at the leading-edges of the wing. In this case the fins act in a vortical flowfield and in general a vortex formation takes place also at the leading-edges of the fins. Over the upper surface an interference between the two vortex systems occurs which determines the pressure distribution and the aerodynamic coefficients.

The basic flow around slender configurations is well known since a long time[1-3]. The arrangement of fins is very close to practical application and therefore systematic investigations are very rare[4-6] or even missing. During the last international conferences on vortical flows[7-9] a lot of control concepts have been discussed. Some papers[10,11] contain aerodynamic coefficients for double-fin configurations, but the corresponding flow phenomena have not been investigated in detail. Characteristic for the lack of knowledge on wing-fin interference are the difficulties with the research aircraft F-18[9,12,13]. Its double fins are located in the vortex field of the leading-edge extension (LEX) and this leads to LEX-vortex breakdown. The double fins act in an unsteady flowfield and experience large oscillations.

In order to develop a basic understanding of the wing-fin interference a slender configuration has been investigated experimentally at low speed. Three different concepts of vertical fin arrangements have been tested on a slender wing:

(i) Central fin, representing the most common fin configuration as used e. g. for the Space-Shuttle Orbiter for which some data are already available[14,15].
(ii) Double fins at about mid semispan position, representing modern fighter aircraft[10-13] as well as the lower stage of the "Sänger" configuration.
(iii) Double fins at the wing tips, representing the "Hermes" as well as the upper stage of the "Sänger" configuration.

Within the basic research program the capabilities of these three concepts are compared. The aerodynamic characteristics are related to the vortex formation and other details of the flowfield around these configurations. This work is an extension of the comprehensive studies at Institut für Strömungsmechanik of Technische Universität Braunschweig on the aerodynamics of slender configurations[1,2,16-20].

2. Nomenclature

2.1 Geometric quantities

$b = 2s$	Wing span
$c(y)$	Local wing chord
$c_t = c(s)$	Wing tip chord
$c_i = c(0)$	Wing central chord
$\bar{c} = \frac{1}{S}\int_{-s}^{+s} c^2(y)dy$	Wing reference chord
$d = d_F$	Thickness of wing and fins
h_F	Hight of fin
n	Exponent (Fig. 2)
$s = b/2$	Wing semispan
x, y, z	Wing-fixed coordinates according to Fig. 1
x^*, z^*	Wing-fixed coordinates normal to the edges of wing and fins, origin at edges
$x_{N25} = \frac{1}{S}\int_{-s}^{+s} c(y)x_{25}(y)dy$	Distance of wing geometric neutral point N_{25} from apex
$x_{25}(y)$	Local quarter chord line of the wing
$y_1(x)$	Local wing semispan (Fig. 3)
$A = b^2/S$	Aspect ratio of the wing
S, S_F	Area of wing, fin
$\delta = d/c_i$	Thickness ratio
ϵ, σ, τ	Dimensionless quantities of Fig. 2, based on c_i
$\xi = x/c_i$, $\eta = y/y_1$	Dimensionless wing-fixed coordinates
$\xi^* = x^*/c_i$, $\zeta^* = z^*/c_i$	Dimensionless wing-fixed coordinates, normal to the edges
φ, φ_F	Leading-edge sweep of wing, fin
$\lambda = c_t/c_i$	Taper ratio of the wing

2.2 Aerodynamic quantities

$c_L = L/q_\infty S$	Lift coefficient
$c_D = D/q_\infty S$	Drag coefficient
$c_Y = Y/q_\infty S$	Side-force coefficient
$c_m = M/q_\infty Sc$	Pitching moment coefficient based on N_{25}, nose-up positive
$c_l = L/q_\infty Ss$	Rolling moment coefficient based on N_{25} according to Fig. 4
$c_n = N/q_\infty Ss$	Yawing moment coefficient based on N_{25} according to Fig. 4
$c_p = (p - p_\infty)/q_\infty$	Pressure coefficient
p	Static pressure
$q_\infty = \rho U_\infty^2/2$	Free stream dynamic pressure
$Re_\infty = U_\infty c_i/\nu$	Reynoldsnumber
U_∞	Free stream velocity

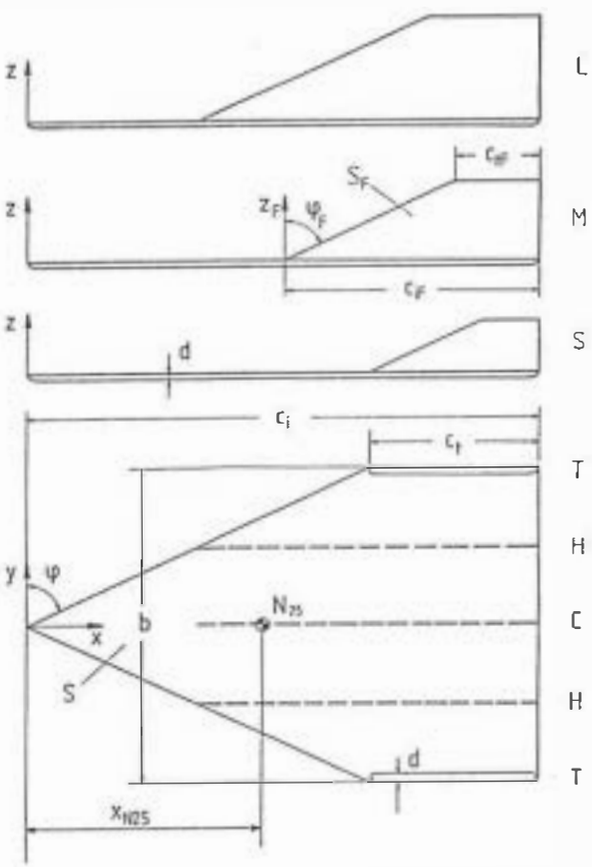

Fig. 1: Cropped delta wing ($A = b^2/S = 0.93$, $\lambda = c_t/c_i = 1/3$, $\varphi = 65°$, flat plate) with half-wing-shaped vertical fins of different size (S, small, $c_{iF}/c_i = 1/3$; M, medium, $c_{iF}/c_i = 1/2$; L, large, $c_{iF}/c_i = 2/3$) in various spanwise positions (C, central; H, half semispan; T, tip).

α	Angle of attack (Fig. 4)
β	Angle of sideslip (Fig. 4)
ν	Kinematic viscosity of air
ρ	Density of air

2.3 Subscripts

F	Fin
W	Wing
∞	Free stream

3. Experimental set-up and test program

The experimental investigations have been carried out in the 1.3 m windtunnel of the Institut für Strömungsmechanik of Technische Universität Braunschweig.

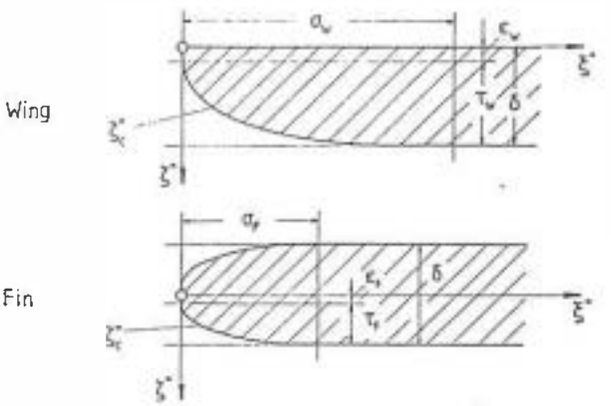

$$\xi^* \le \sigma_{W,F} : \zeta_C^* = \tau_{W,F}\left[1 - \left[\frac{\sigma_{W,F} - \xi^*}{\sigma_{W,F}}\right]^3\right]^n + \epsilon_{W,F}$$

$$\xi^* > \sigma_{W,F} : \zeta_C^* = \tau_{W,F} + \epsilon_{W,F}$$

Section normal to	$\sigma_W = 2\sigma_F$	$\epsilon_W = 2\epsilon_F$	$\tau_W = 2\tau_F$	n
trailing-edge	7/120	1/600	1/120	1
side-edge	1/24	1/600	1/120	1/2
leading-edge	$\frac{7\cos 65°}{120}$	1/600	1/120	1

Fig. 2: Details of the shapes of the edges of wing and fins.

3.1 Windtunnel model

The windtunnel model according to Fig. 1 consists of a cropped delta wing with an aspect ratio A = 0.93. Its leading-edge sweep $\varphi = 65°$ is the same as for the configuration of the International Vortex Flow Experiment (VFE)[2]. The taper ratio has been chosen as $c_t/c_i = 1/3$ in order to provide a sufficient size of wing tip mounted fins. Half-wing shaped vertical fins of different size (S small, M medium, L large) were used and they were positioned at the trailing-edge of the wing in three spanwise positions (C central single, H mid semispan twin and T tip twin). All combinations of size and position were tested with the exception that in the wing-tip position only the small fins were possible. Wing and fins were manufactured as thin flat plates of constant thickness ratio $\delta = d/c_i = 1/100$. All edges have been rounded unsymmetrically from the lower side for the wing and symmetrically for the fins. Details are given in Fig. 2. Considering the very small thickness of wing and fins in spite of a certain bluntness the edges may be regarded as aerodynamically sharp. The model size was $c_i = 600$ mm.

The wing and the fins are equipped with a tube system underneath the surface in order to measure the pressure distribution. The location of the tubes and the positions of the taps may be taken from Fig. 3.

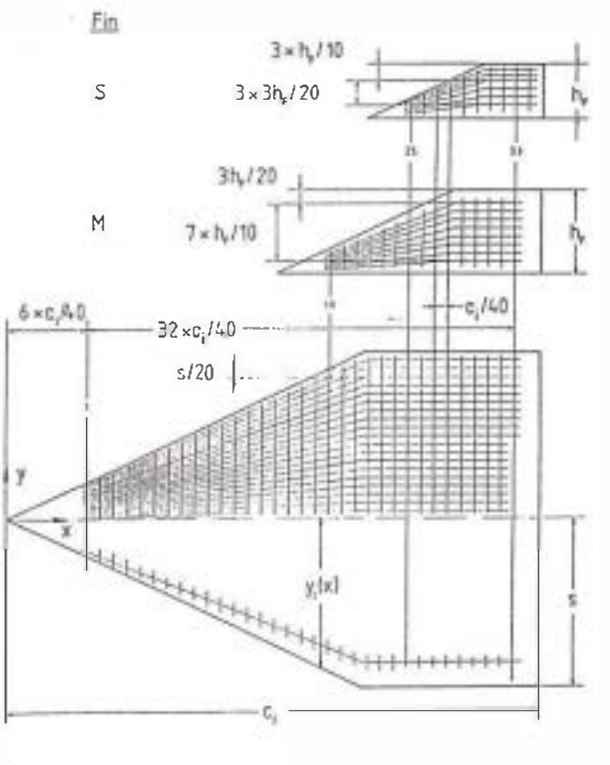

Fig. 3: Positions of the pressure taps on the wing and on the fins M and S.

3.2 Test program

All measurements have been carried out for a free-stream velocity of $U_\infty = 34$ m/s, which corresponds to a Reynoldsnumber based on c_i of $Re_\infty = U_\infty \cdot c_i/\nu = 1.4 \cdot 10^6$.

For the wing alone as well as for all 7 possible wing-fin combinations (SC, SH, ST, MC, MH, LC, LH) six-component balance measurements have been carried out for

$$-5° \leq \alpha \leq 40° \text{ and } -7.5° \leq \beta \leq 26.0°.$$

The aerodynamic coefficients have been evaluated with respect to the experimental coordinate system located in the geometric neutral point N_{25} of the wing according to Fig. 4.

Pressure distribution measurements have been performed for the wing alone W and for the configurations SH, ST and MC only. The latter are very well suited for comparison between each other: For the medium-sized fin M the area ratio is $S_F/S = 1/4$ and for the two other configurations with two small sized fins S the total area ratio is $2S_F/S = 2/9 = 1/4.5$. This means that the effective fin area is about the same for all three wing-fin conifgurations. The pressure distribution measurements have been carried out for the angles of attack

$$\alpha = 10°, (15°), 20°, 25°, 30°, (35°), 40° \qquad (1)$$

and for the angles of sideslip

$$\beta = 0°, 5°, 10°, 15°, 20°, \qquad (2)$$

where the values in brackets have been investigated for the wing alone only.

The flowfield has been studied qualitatively by means of the Laser lightsheet technique for the free stream directions according to equ. (1) and (2). The Laser lightsheet has been adjusted perpendicular to the free-stream and moved through the flowfield using the traversing device of the LDA-system of the windtunnel. The flow situation within the Laser lightsheet has been documented from behind by a video camera. Additional flow visualizations have been carried out on the surface by means of oilflow patterns. The corresponding test program was

$$\alpha = 10°, 20°, 30°, 40° \qquad (3)$$

and $\beta = 0°, 10°, 20°$.

In these investigations the black upper surface of the wing and of both sides of the fins were painted by a mixture of melamine-sulfonamite-formaldehyde-resin powder and petroleum and benzine (ratio of components: 1 g powder : 3 cm³ petroleum : 1 cm³ benzine) and exposed to the flow for about half a minute.

Flowfield measurements using a 2 mm 5-hole probe have been carried out for the wing alone as well as for the configuration ST with two small tip-mounted fins at $\alpha = 13.5°$. Three wing-fixed cross-sections at $x/c_i = 0.70/0.85/1.01$ have been chosen in which the total pressure distribution as well as the local velocity vector have been determined.

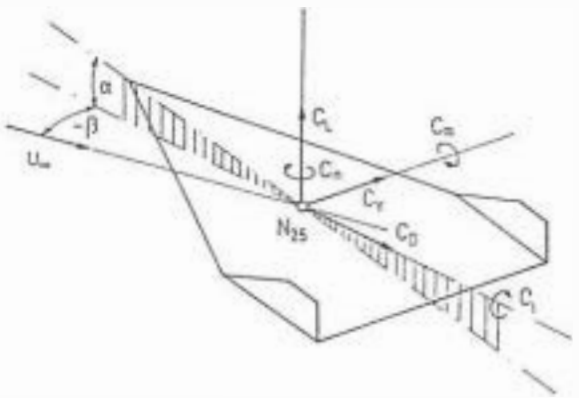

Fig. 4: Experimental coordinate system for windtunnel data reduction.

4. Results

Some typical results of the six-component measurements for the wing alone (W) as well as for the configurations (MC), (SH) and (ST) are shown in Figs. 5 to 7. Fig. 5 contains aerodynamic coefficients in symmetrical flow and in Fig. 6 the derivatives $c_{l\beta}$, $c_{n\beta}$ and $c_{Y\beta}$ of the lateral motion are given and Fig. 7 shows some peculiarities which occur at large angles of attack in unsymmetrical flow. The corresponding flow situations will be discussed subsequently by means of some characteristic pressure distributions as well as by surface oilflow patterns.

4.1 Wing alone

The well-known nonlinear dependence of the aerodynamic coefficients on the angle of attack turns out for small and medium angles of attack. At $\alpha = 20°$ vortex breakdown takes place over the wing and the lift and nose-down pitching moment coefficients are reduced as indicated in Fig. 5 by hatching. In unsymmetrical flow at moderate angles of attack the wing vortex system moves leewards. The windward vortex is stronger than the one on the leeward side and this leads to stable contributions to the derivatives of the lateral motion according to Fig. 6. Unsymmetrical vortex breakdown reduces the suction on the windward side and this causes a reduction of the stable rolling and yawing moment derivatives as indicated in Fig. 6 by hatching. This behaviour of the wing is in excellent agreement with data from the literature[2].

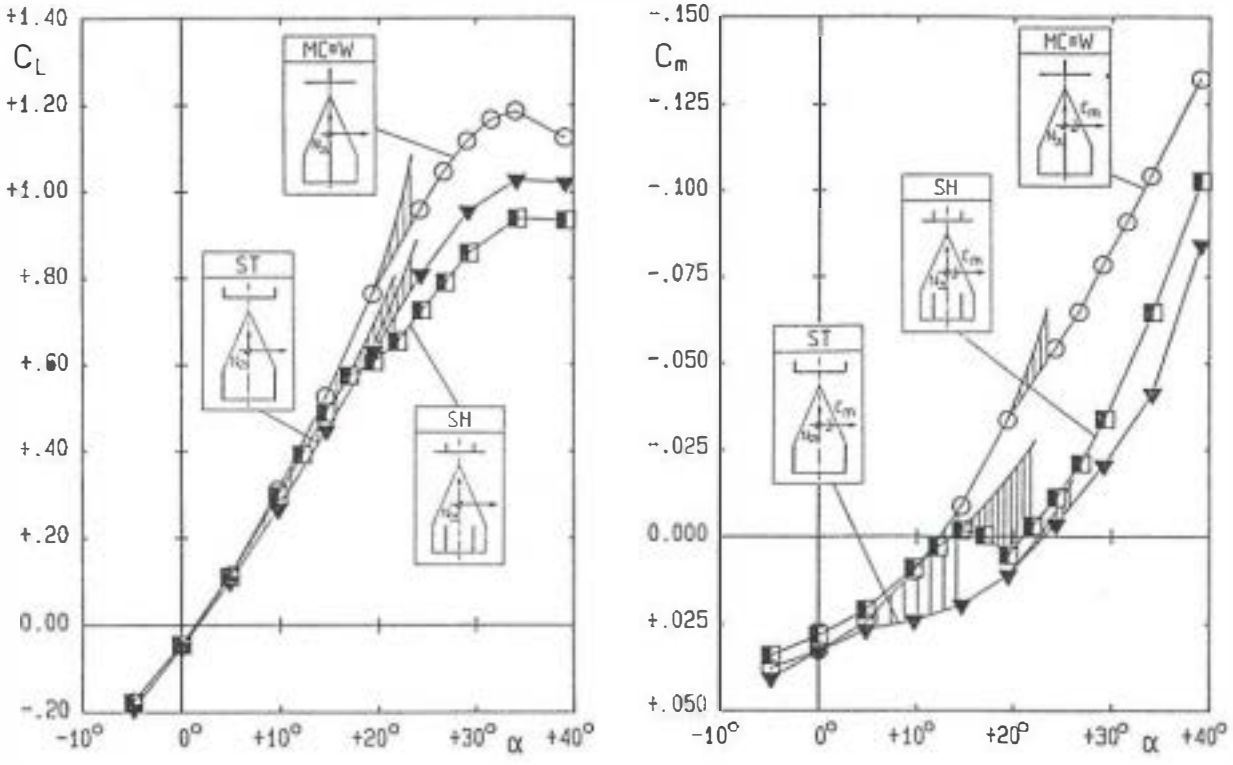

Fig. 5: Lift and pitching moment characteristics for the wing alone W and the wing-fin configura tions MC, SH, ST in symmetrical flow.

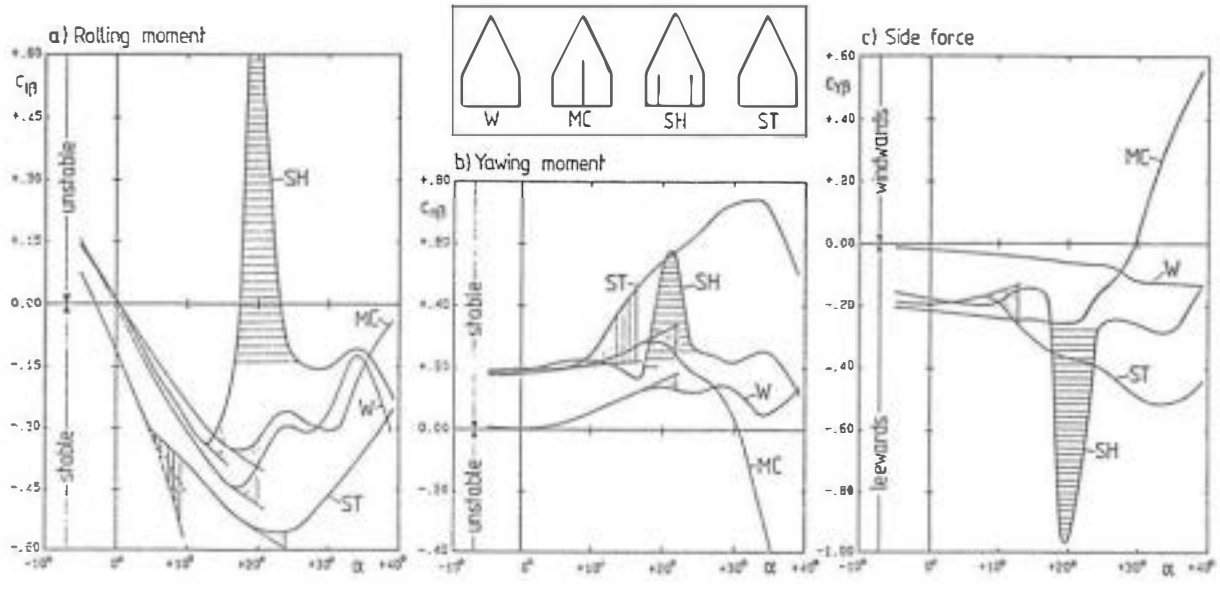

Fig. 6: Stability derivatives of the lateral motion for the wing alone W and the wing-fin configurations MC, SH, ST. Fine vertical hatching: effect of vortex breakdown, coarse vertical hatching: effect of fin vortex formation, horizontal hatching: region of high instability.

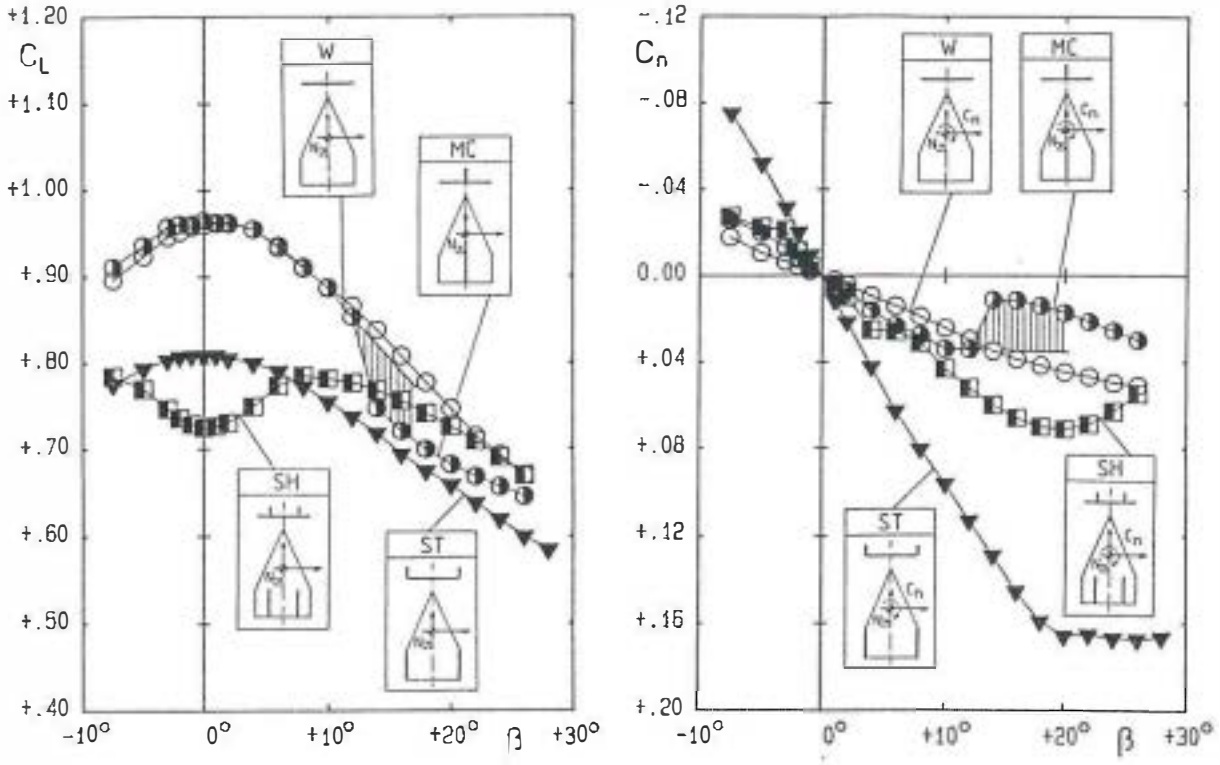

Fig. 7: Lift and yawing moment characteristics for the wing alone W and the wing-fin configurations at $\alpha = 25°$.

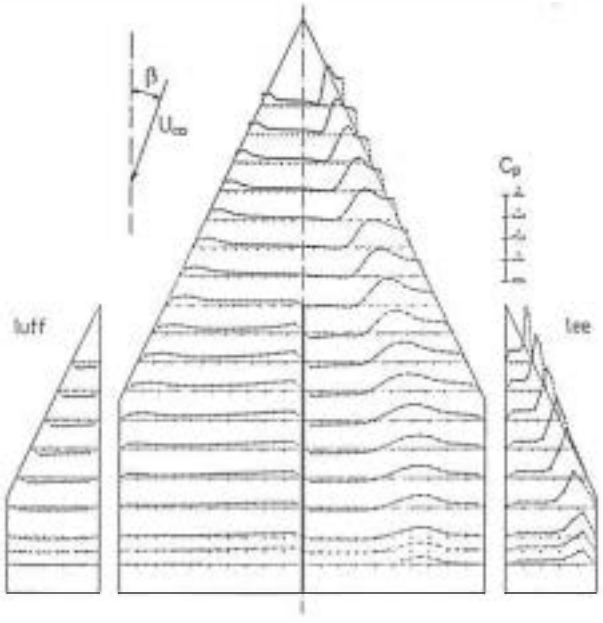

Fig. 8: Pressure distribution on the wing-fin configuration MC at $\alpha = 10°$, $\beta = 20°$.

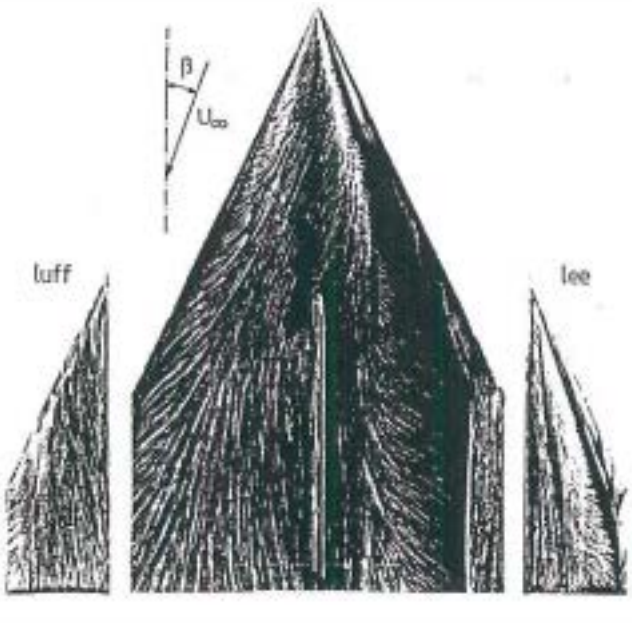

Fig. 9: Surface oilflow pattern on the wing-fin configuration MC at $\alpha = 10°$, $\beta = 20°$.

4.2 Wing with central fin

The lift and pitching moment characteristics in symmetrical flow are the same for the wing alone (W) and for the configuration (MC) under consideration. In unsymmetrical flow the central fin yields a stabilizing contribution to the yawing moment and sideforce derivatives according to Fig. 6. A typical pressure distribution is shown in Fig. 8. On the fin occur high pressures on the windward side and low pressures associated with a fin-vortex formation on the leeward side. This means that from the fin results also a stabilizing contribution to the rolling moment derivative, but the pressure distributions indicate, that from the inner portions of the wing originates a counter-acting rolling moment, which is predominant and which reduces the overall rolling moment derivative c_{l_β} (Fig. 6).

Fig. 8 demonstrates that for moderate values of the angle of attack and the angle of sideslip the central fin is located between the two attachment lines of the wing vortices. The flow separates from the leading-edge of the fin and a concentrated vortex occurs on the lee-side of the fin. At a large angle of attack $\alpha = 25°$, however, the configuration (MC) shows sudden changes of lift and yawing moment at a certain angle of sideslip (Fig. 7). Corresponding pressure distributions at $\alpha = 25°$ for different angles of sideslip are given in Figs. 10 and 11. Between $\beta = 10°$ (Fig. 10) and $\beta = 20°$ (Fig. 11) the central fin suddenly enters the flowfield of the vortex on the windward side of the configuration. The attachment line of this vortex switches to the leeward side of the fin. At $\beta = 10°$ (Fig. 10) vortex breakdown is already present in the vortex on the windward side of the wing, but the additional disturbance of the windward vortex by the fin at $\beta = 20°$ (Fig. 11) suddenly causes increased vortex breakdown there. Aside the fin a deadwater-type flow with constant static pressure is present which leads to an abrupt loss of lift and a reduction of the stable yawing moment. These effects are indicated in Fig. 7 by hatching.

4.3 Wing with double fin at mid semispan

For small angles of attack on configuration (SH) the wing vortices are located outside the fins. At $\alpha \approx 12°$ the attachment line of the wing vortices switches to the inner side of the fins and this leads to flow separations on the outer side of the fins. The disturbance caused by the fins produces earlier vortex breakdown with increasing angle of attack (Fig. 5) and this is the reason for the low maximum lift coefficient of configuration (SH).

The stability derivatives of the lateral motion according to Fig. 6 show extremely unstable rolling moments as well as stable sideforces and yawing moments in the vicinity of an angle of attack of $\alpha \approx 20°$. The symmetrical flow at this angle of attack is analyzed in Fig. 12. The attachment line of the wing vortex is located on the inner side of the fin and a fin vortex is formed over the outer surface of the fin. Vortex breakdown takes place within the wing vortices at about $x/c_i = 0.6$. This flowfield is very

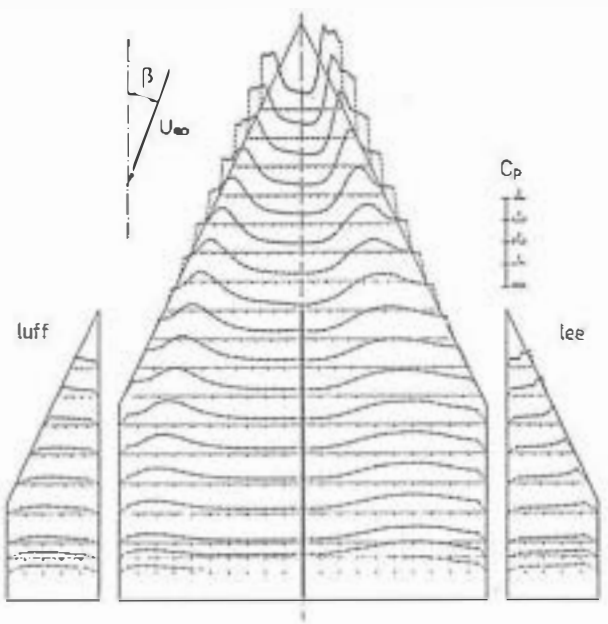

Fig. 10: Pressure distribution on the wing-fin configuration MC at $\alpha = 25°$, $\beta = 10°$.

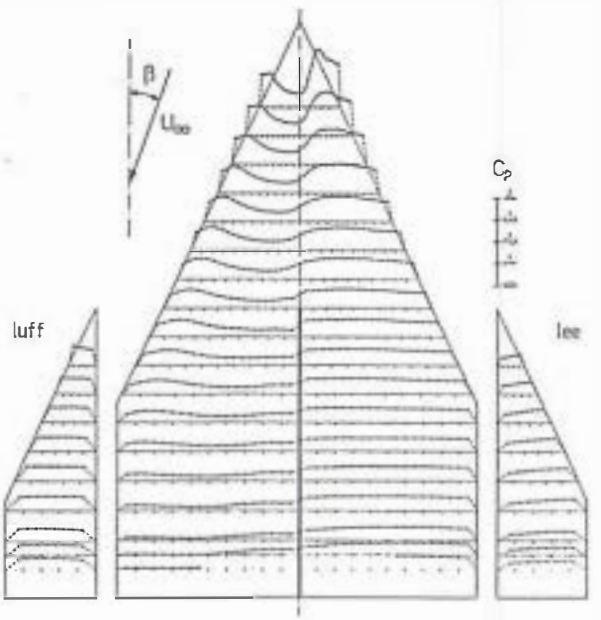

Fig. 11: Pressure distribution on the wing-fin configuration MC at $\alpha = 25°$, $\beta = 20°$.

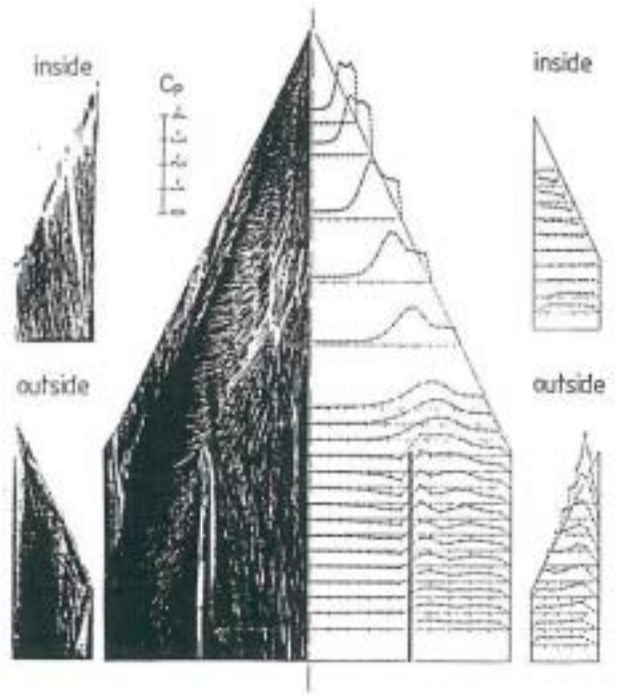

Fig. 12: Pressure distribution and surface oilflow pattern on the wing-fin configuration SH at α = 20°, β = 0° (Oilflow patterns from the fin enlarged).

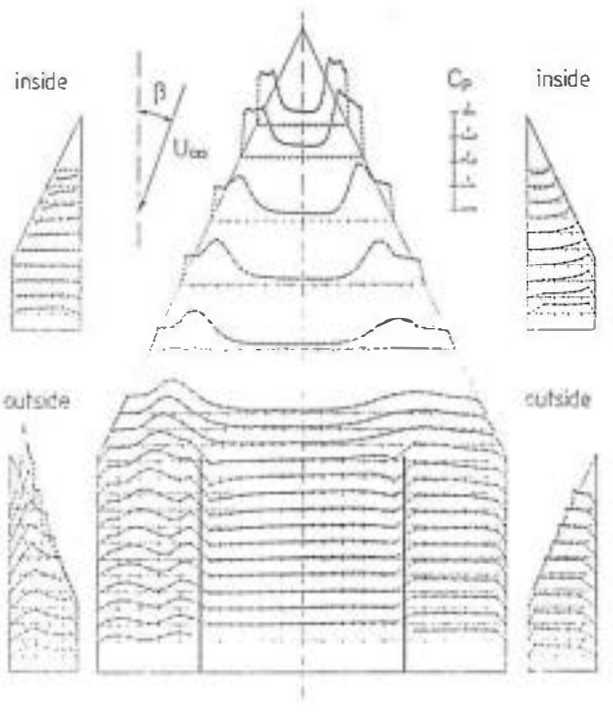

Fig. 13: Pressure distribution on the wing-fin configuration SH at α = 20°, β = 5°.

sensitive with respect to changes in the free-stream conditions.

For a small angle of sideslip according to Fig. 13 and Fig. 14a on the leeward side of the configuration the fin vortex is weakened due to reduced crossflow acting on the fin and the flow status remains in principle the same as in symmetrical flow, but due to the reduction of the disturbance from the fin, vortex breakdown is delayed within the wing vortex. On the windward side of the configuration, however, the fin cuts deeply into the wing vortex. The crossflow around the fin is increased and the combination of vortex breakdown within the wing vortex and vortex breakdown within the fin vortex leads to a deadwater-type flow between the fin and the wing tip. This heavy disturbance causes very early vortex breakdown of the wing vortex on the windward side and the corresponding reduction of the suction leads to the extremely unstable rolling moments according to Fig. 5, whereas the stable yawing moment and sideforce derivatives result from the corresponding pressure distributions on the two fins.

The flow state according to Fig. 12 is also very sensitive with respect to the angle of attack. If it is slightly increased to $\alpha > 20°$ the wing-vortex-induced crossflow at the fins is so strong that already in symmetrical flow the deadwater-type flow between the fin and the wing tip establishes on both sides simultaneously. Fig. 14b shows an example for such a flow situation at α = 30°, β = 0°. If a small angle of sideslip is added the deadwater-type flow structure between the fin and the wing tip remains the same on both sides. On the other hand if for the highly unstable situation at a small angle of sideslip and α = 20° the angle of attack is slightly increased to $\alpha > 20°$, the deadwater-type flow between fin and wing tip occurs also on the leeward side of the configuration. If the same flow structures are

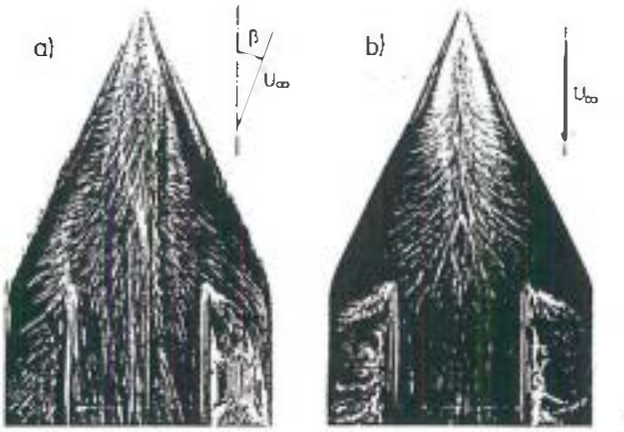

Fig. 14: Surface oilflow pattern on the wing of the wing-fin configuration SH at
a) α = 20°, β = 10° and b) α = 30°, β = 0°.

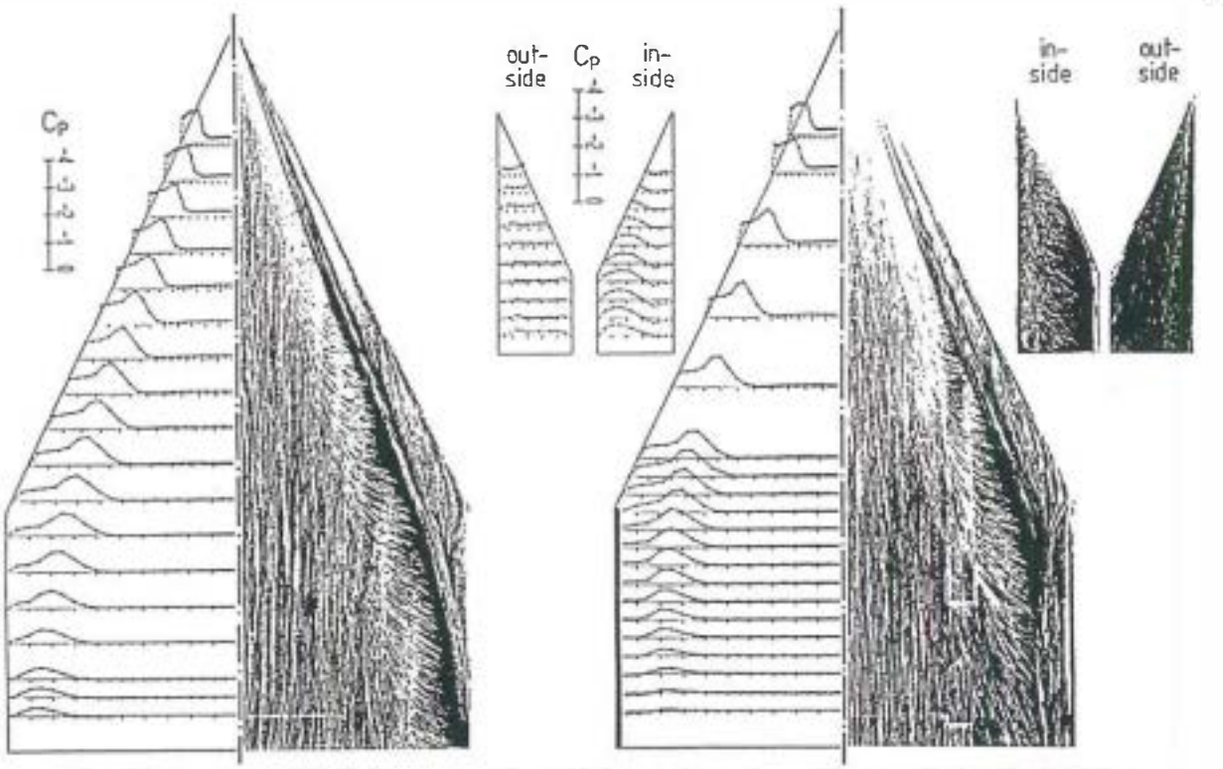

Fig. 15: Pressure distribution and surface oilflow pattern at $\alpha = 10°$, $\beta = 0°$ for a) Wing alone (W) and b) Wing-fin configuration ST (Oilflow patterns from the fin enlarged).

present on both sides the configuration is stable in roll. For very large angles of sideslip the vortical flow between fin and wing tip is restored. This leads to a destabilization but not to an instability in roll.

In conclusion, for the configuration (SH) in symmetrical flow $\beta = 0°$ between the fins and the wing tips a vortical flow is present for $\alpha < 16°$ and a deadwater-type flow for $\alpha > 24°$ on both sides, even for small angles of sideslip, and the configuration is stable in roll. In the angle of attack range $16° < \alpha < 20°$ small angles of sideslip lead to an unsymmetrical formation of deadwater-type flow between the fin and the wing tip which causes high instability in roll. For angles of attack $20° < \alpha < 24°$ the deadwater-type flow establishes also on the leeward side of the configuration and stability in roll is recovered.

4.4 Wing with double fin at the wing tips

4.4.1 Forces, moments, pressure distributions and surface flow

The three-component measurements on the configuration (ST) according to Fig. 5 indicate about the same vortex breakdown location as for the wing alone (W), but lift and nose-down pitching moment are smaller than for the wing alone. Fig. 15 shows the pressure distributions on the upper surface for the wing alone (W) and for the wing-fin configuration (ST) at $\alpha = 10°$ and $\beta = 0°$. A comparison for the same sections $\xi = \text{const.}$ yields significantly lower suction for the configuration (ST) as compared with the wing alone (W). The reason for this is the fact that flow separation and vortex formation along the leading-edge of the wing continues along the leading-edge of the vertical fins, and this leads to a vortex on each side of the configuration (ST) which is located higher than on the wing alone (W). Correspondingly lift and nose-down pitching moment are lower than for the wing alone (W), see Fig. 5. The pressure distributions and the oilflow patterns according to Fig. 15 indicate the suction of the wing vortex on the inner surface of the fin as well as the formation of a small vortex on the outer surface of the fin which is due to flow separations at the lower edge of the fin.

In unsymmetrical flow the sideforce and yawing moment derivatives on the configuration (ST) are in the same order of magnitude as for the other fin configurations (Fig. 6). The rolling moment derivative, however, is shifted towards more stable values. This is an effect of the fins which is not present in the other configurations: In the case of tip mounted fins the stable rolling moment contribution from the

fins is not compensated by a counter-acting contribution from the wing. In Fig. 16 a typical pressure distribution at $\alpha = 10°$, $\beta = 20°$ is given and Fig. 17 shows the corresponding oilflow patterns. The fins produce stable rolling moment contributions, and outside the fins there exists no wing and the interference between the fins and the inner portions of the wing leads to a stable contribution from the wing too. Another reason for the high lateral stability of the configuration (ST) are the flow separations in the lower part of the fins, mentioned above. In unsymmetrical flow the vortex on the outer surface of the windward fin is reduced whereas the one on the leeward fin is increased. This leads to an additional sideforce in leeward direction and to stable rolling and yawing moment contributions, marked in Fig. 6 by coarse vertical hatching. The raise of the wing vortices in the region of the fins has also a consequence in unsymmetrical flow. The rolling moment contribution from the wing is reduced and this effect compensates the stabilizing contribution from the fins as indicated in Fig. 5a. Sideforce and yawing moment are not significantly influenced by this effect. At angles of attack $\alpha > 20°$ unsymmetrical vortex breakdown leads to the well-known loss of stability concerning the rolling moment whereas sideforce and yawing moment experience only minor contributions from this flow situation.

4.4.2 Vortical flowfield

In the case of wing tip mounted vertical fins the leading-edge separation continues from the wing to the fin. However, the wing-vortex induced local crossflow at the leading-edge of the fin is directed outwards and this means that counter-rotating vorticity should be shed along the leading-edge of the fin. In order to check this situation flowfield measurements have been carried out in two planes perpendicular to the wing at $\xi = 0.85$ well downstream of fin apex and upstream of the end of the fin leading-edge as well as at the trailing-edge $\xi = 1.01$ of the configuration. The result is shown in Fig. 18 by means of total pressure and axial vorticity contours in both planes at $\alpha = 13.5°$, $\beta = 0°$. At $\xi = 0.85$ the total pressure contours indicate the wing vortex as well as a second vortex just above the vertical fin and a third vortex on the outer surface of the fin close to the lower edge. The corresponding axial vorticity contours show, that the third vortex has the same sense of rotation as the wing vortex as expected from the flow separation at the lower edge of the fin. The vortex on top of the fin, however, is counter-rotating with respect to the wing primary vortex. This indicates that along the leading-edge of the fin vorticity is shed with the sense of rotation opposite to that along the leading-edge of the wing.

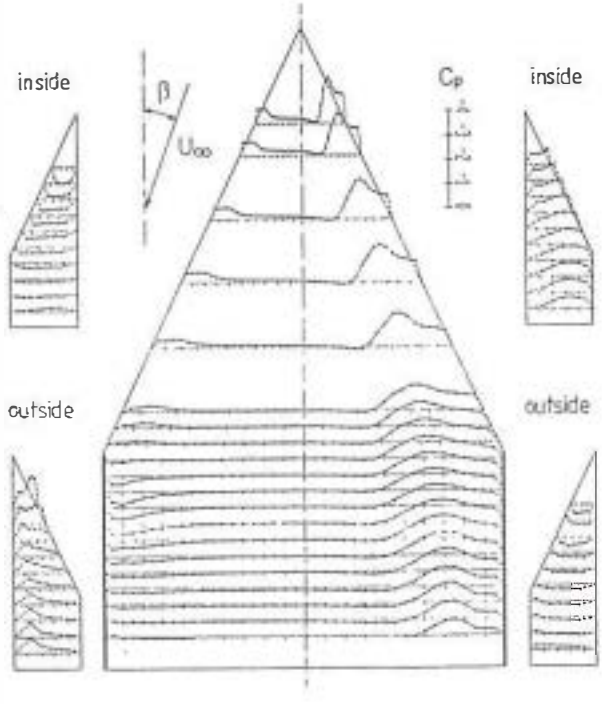

Fig. 16: Pressure distribution on the wing-fin configuration ST at $\alpha = 10°$, $\beta = 20°$.

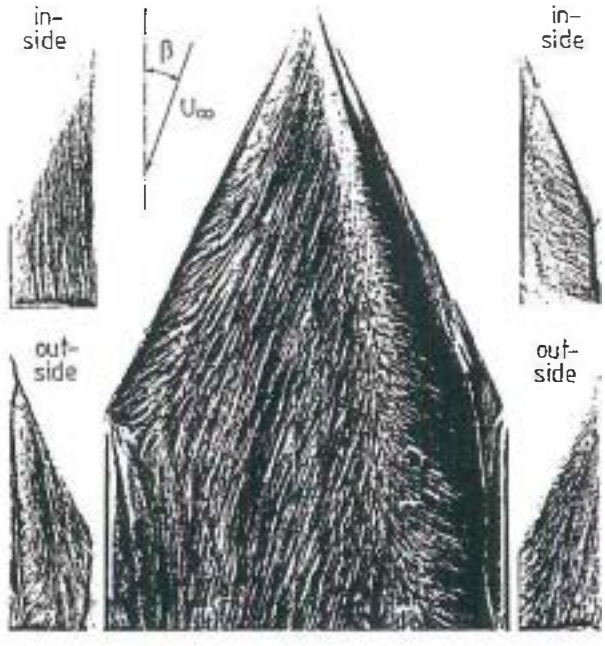

Fig. 17: Surface oilflow pattern on the wing-fin configuration ST at $\alpha = 10°$, $\beta = 20°$ (Oilflow patterns from the fins enlarged).

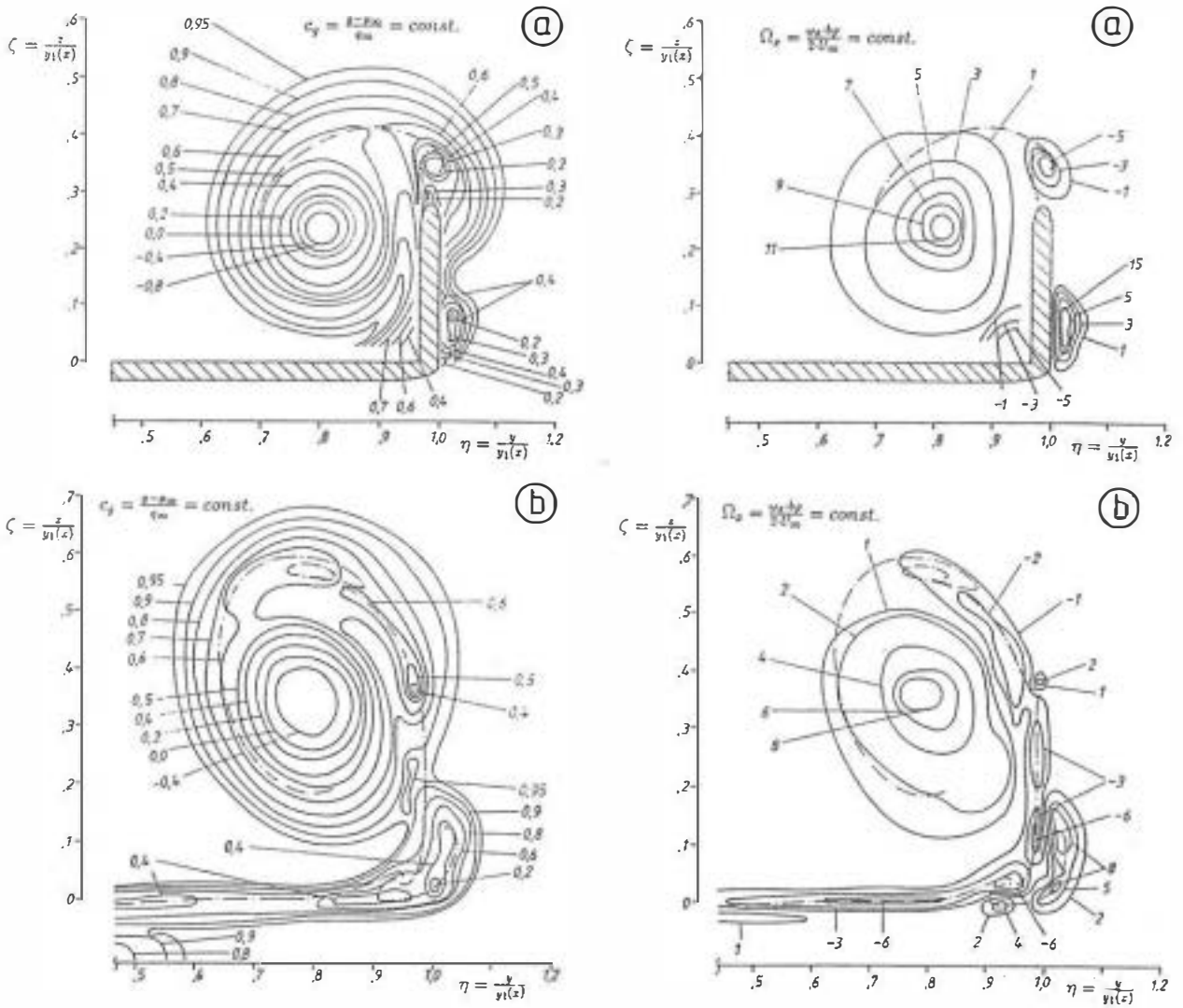

Fig. 18: Flowfield on the wing-fin configuration ST at $\alpha = 13.5°$, $\beta = 0°$ in cross-sections at a) $\xi = 0.85$ and b) $\xi = 1.01$. Lines of constant total pressure lefthand and lines of constant axial vorticity righthand.

At the trailing-edge the situation is much more complicated. The wing primary vortex is again marked by considerable total pressure losses and by a large amount of positive axial vorticity. The counter-rotating vortex from the leading-edge of the fin is no longer present in concentrated form. Negative axial vorticity is found only in a certain band at the upper periphery of the wing vortex. Increased total pressure losses in combination with positive axial vorticity in the tip region of the fin might indicate that near the trailing-edge vorticity is shed from the fin which has again the same sense of rotation as the primary wing vortex. The wakes of wing and fin contain a considerable amount of negative axial vorticity. This is well known from delta wings[1, 2] and it can be expected that trailing-edge vortices will develop in the wake downstream of the wing and the fin. The vortex sheet of the fin vortex at the bottom of the fin must be connected with the wing-fin trailing vortex sheet. This leads to the formation of a triple-branched vortex which rotates opposite to the wing primary vortex (negative axial vorticity) and which is located right in the corner between wing and fin. Further studies of this complicated vortex formation are necessary.

4.5 Concluding discussion

A comparison of the three concepts (MC), (SH) and (ST) for vertical fins on the basis of the present investigations leads to the following conclusions:

a) A central fin configuration (MC) reaches the highest maximum lift coefficients. Up to moderate angles of attack lateral stability is present in the vicinity of the symmetrical flow state. For flight in sideslip at high angles of attack, however, sudden changes in the aerodynamic derivatives occur and lateral stability is considerably reduced.
b) Configurations with double fins in a mid-semispan position (SH) are very unfavourable. They reach only low values for the maximum lift coefficient and in a certain angle of attack range they are extremely unstable in roll.
c) Configurations with double fins in wing tip position (ST) are favourable in general. They are laterally stable for all free-stream conditions and further improvements are possible by means of sharp lower edges of the fins which support the formation of fin vortices and lead to an increase in lateral stability. Their only disadvantage is a certain loss of lift in comparison with the wing alone (W) due to a slight upwards shift of the wing vortex system.

The corresponding flow states have been documented by means of pressure distributions, oilflow patterns and flowfield measurements. In these investigations the following principles have been found:

d) As long as the fins are located between the attachement lines of the wing vortices the wing fin interference is weak.
e) If the attachement line of a wing vortex switches to the inner surface of a fin, strong wing fin interference takes place. In this case:
f) The fin causes increased wing vortex breakdown and
g) The fin experiences a wing vortex induced cross-flow which leads to flow separations at the fin either of vortical type or of deadwater type. The corresponding fin vortex system interferes with the wing vortex system.
h) Along the leading-edges of tip mounted vertical fins vorticity is shed, the rotation of which is opposite to that of the primary wing vortex on the respective side.

In general the present investigations suggest the following interference mechanism: If a flat plate (vertical fin) is traversed through a (wing-) vortex the vortex is not divided in parts but the disturbance by the plate leads to vortex breakdown. This means that the vortex switches from one side of the plate to the other through the intermediate state of vortex breakdown.

References

[1] D. Hummel: On the vortex formation over a slender wing at large angles of incidence. AGARD-CP-247 (1978), 15-1 to 15-17.

[2] D. Hummel: Documentation of separated flows for computational fluid dynamics validation. AGARD-CP-437 (1988), Vol. 2, P 15-1 to P 15-24.

[3] G. Drougge: The international vortex flow experiment for computer code validation. ICAS-Proceedings 1988, Vol. 1, XXXV - XL1.

[4] W. H. Wentz, Jr.: Vortex-fin interaction on a fighter aircraft. AIAA Paper 87 - 2474 (1987).

[5] A. E. Washburn, L. N. Jenkins, M. A. Ferman: Experimental investigation of vortex-fin interaction. AIAA Paper 93-0050 (1993).

[6] S. H. Krist, A. E. Washburn, D. Visser: A computational and experimental investigation of a delta wing with vertical tails. AIAA Paper 93-3009 (1993).

[7] AGARD (Ed.): Aerodynamics of vortical type flows in three dimensions. AGARD-FDP Symposium Rotterdam 1983, AGARD-CP-342 (1983).

[8] AGARD (Ed.): Aerodynamics of combat aircraft controls and of ground proximity. AGARD-FDP Symposium Madrid 1989, AGARD-CP-465 (1990).

[9] AGARD (Ed.): Vortex flow aerodynamics. AGARD-FDP Symposium Scheveningen 1990, AGARD-CP-494 (1991).

[10] W. P. Gilbert, L. T. Nguyen, J. Gera: Control research in the NASA high-alpha technology program. AGARD-CP-465 (1990), 3-1 to 3-18.

[11] B. A. Marks, D. E. Hahne: Innovative control concepts and component integration for a generic supercruise fighter. AGARD-CP-465 (1990), 10-1 to 10-14.

[12] C. A. Martin, D. H. Thompson: Scale model measurements of fin buffet due to vortex bursting on F/A-18. AGARD CP-497 (1992), Paper No. 12.

[13] B. H. K. Lee, D. Brown: Wind-tunnel studies of F/A-18 tail buffet. J. Aircraft 29 (1992), 146 - 152

[14] W. E. Bornemann, T. E. Surber: Aerodynamic design of the Space-Shuttle Orbiter. AGARC-CP-247 (1978), 11-1 to 11-24.

[15] D. C. Freeman: Dynamic stability derivatives of Space Shuttle Orbiter obtained from wind-tunnel and approach and landing flight tests. NASA-TN 1634 (1980), 1 - 17.

[16] D. Hummel, H.-Chr. Oelker: Effects of canard position on the aerodynamic characteristics of a close-coupled canard configuration at low speed. AGARD-CP-465 (1989), 7-1 to 7-18. See also Z. Flugwiss. Weltraumforsch. 15 (1991), 74 - 88.

[17] H.-Chr. Oelker, D. Hummel: Investigations on the vorticity sheets of a close-coupled delta-canard configuration. J. Aircraft 26 (1989), 657 - 666.

[18] A. Bergmann, D. Hummel, H.-Chr. Oelker: Vortex formation over a close-coupled canard-wing-body configuration in unsymmetrical flow. AGARD-CP-494 (1991), 14-1 to 14-14.

[19] D. Hummel, H.-Chr. Oelker: Low-speed characteristics for the wing-canard configuration of the international vortex flow experiment (to be published in J. Aircraft).

[20] A. Brümmer, D. Hummel: Aerodynamische Eigenschaften eines schlanken Flügels mit Seitenleitwerken im Niedergeschwindigkeitsbereich. Jb. Dtsch. Ges. Luft- u. Raumf. 1992, 227 - 236.